The First Solution Structure of a Paramagnetic Copper(II) Protein: The Case of Oxidized Plastocyanin from the Cyanobacterium *Synechocystis* PCC6803

Ivano Bertini,[†] Stefano Ciurli,[‡] Alexander Dikiy,[‡] Claudio O. Fernàndez,[†,⊥] Claudio Luchinat,[§] Niyaz Safarov,[‡] Sergiy Shumilin,[†] and Alejandro J. Vila[‖]

Contribution from the Magnetic Resonance Center, University of Florence, Via L. Sacconi, 6, 50019 Sesto Fiorentino, Italy, Department of Agro-Environmental Science and Technology, University of Bologna, Viale Berti Pichat 10, 40127 Bologna, Italy, Department of Agricultural Biotechnology, University of Florence, P.le delle Cascine 18, 50144 Florence, Italy, Biophysics Section, Department of Biological Chemistry, University of Rosario, Suipacha 531, 2000 Rosario, Argentina, and LANAIS RMN 300 (UBA-CONICET), Junin 956, 1113 Buenos Aires, Argentina

Abstract: The NMR solution structure of oxidized plastocyanin from the cyanobacterium *Synechocystis* PCC6803 is here reported. The protein contains paramagnetic copper(II), whose electronic relaxation times are quite unfavorable for NMR solution studies. The structure has been solved on the basis of 1041 meaningful NOESY cross-peaks, 18 1D NOEs, 26 T_1 values, 96 dihedral angle constraints, and 18 H-bonds. The detection of broad hyperfine-shifted signals and their full assignment allowed the identification of the copper(II) ligands and the determination of the Cu−S−C−H dihedral angle for the coordinated cysteine. The global root-mean-square deviation from the mean structure for the solution structure family is 0.72 ± 0.14 and 1.16 ± 0.17 Å for backbone and heavy atoms, respectively. The structure is overall quite satisfactory and represents a breakthrough, in that it includes paramagnetic copper proteins among the metalloproteins for which solution structures can be afforded. The comparison with the available X-ray structure of a triple mutant is also performed.

Introduction

Plastocyanins are small (∼10 kDa) soluble proteins involved in electron-transfer processes occurring during photosynthesis.[1−3] Plastocyanins belong to a larger class of metalloproteins, named blue copper proteins, containing Cu in the active site.[4−6] Several structural models of plastocyanins from different biological sources are available, most of which refer to solid-state crystallographic structures of either oxidized or reduced forms, containing, respectively, Cu(II) and Cu(I).[7−17] On the other hand, all available solution structures of plastocyanins determined by NMR refer to the reduced Cu(I) diamagnetic form of the protein.[18−21] The unavailability of solution structures of oxidized plastocyanins is certainly due to the intrinsic difficulties embedded in the NMR characterization of the Cu(II)-containing form, in turn caused by the peculiar magnetic properties of the oxidized copper ion. In particular, Cu(II) is a d^9 open-shell transition-metal ion possessing an unpaired electron ($S = 1/2$). The long electronic relaxation time featured by tetragonal copper(II)[22] causes very large line widths for the ^1H NMR signals of the amino acid residues located in the vicinity of the metal ion. In this context, the situation is somewhat better for plastocyanins, characterized by the presence of a copper ion strongly bound to two histidines and one cysteine in a distorted trigonal geometry (N_2S coordination), in addition to a fourth

† Magnetic Resonance Center, University of Florence.
‡ University of Bologna.
§ Department of Agricultural Biotechnology, University of Florence.
‖ University of Rosario.
⊥ LANAIS RMN 300 (UBA-CONICET).
(1) Redinbo, M. R.; Yeates, T. O.; Merchant, S. *J. Bioenerg. Biomembr.* **1994**, *26*, 49−66.
(2) Navarro, J. A.; Hervàs, M.; De la Rosa, M. A. *J. Biol. Inorg. Chem.* **1997**, *2*, 11−22.
(3) Hope, A. B. *Biochim. Biophys. Acta* **2000**, *1456*, 5−26.
(4) Adman, E. T. *Adv. Protein Chem.* **1991**, *42*, 144−197.
(5) Sykes, A. G. *Struct. Bonding* **1991**, *75*, 175−224.
(6) Malmstrom, B. G. *Eur. J. Biochem.* **1994**, *223*, 711−718.
(7) Guss, J. M.; Freeman, H. C. *J. Mol. Biol.* **1983**, *169*, 521−563.
(8) Guss, J. M.; Harrowell, P. R.; Murata, M.; Norris, V. A.; Freeman, H. C. *J. Mol. Biol.* **1986**, *192*, 361−387.
(9) Collyer, C. A.; Guss, J. M.; Sugimura, Y.; Yoshizaki, F.; Freeman, H. C. *J. Mol. Biol.* **1990**, *211*, 617−632.
(10) Guss, J. M.; Bartunik, H. D.; H. C., F. *Acta Crystallogr.* **1992**, *B48*, 790−811.
(11) Redinbo, M. R.; Cascio, D.; Choukair, M. K.; Rice, D.; Merchant, S.; Yeates, T. O. *Biochemistry* **1993**, *32*, 10560−10567.
(12) Xue, Y.; Okvist, M.; Hansson, O.; Young, S. *Protein Sci.* **1998**, *7*, 2099−2105.
(13) Romero, A.; De la Cerda, B.; Vareda, P. F.; Navarro, J. A.; Hervas, M.; De la Rosa, M. A. *J. Mol. Biol.* **1998**, *275*, 327−336.
(14) Sugawara, H.; Inoue, T.; Li, C.; Gotowda, M.; Hibino, T.; Takabe, T.; Kai, Y. *J. Biochem. (Tokyo)* **1999**, *125*, 899.
(15) Inoue, T.; Sugawara, H.; Hamanaka, S.; Tsukui, H.; Suzuki, E.; Kohzuma, T.; Kai, Y. *Biochemistry* **1999**, *38*, 6063−6069.
(16) Bond, C. S.; Bendall, D. S.; Freeman, H. C.; Guss, J. M.; Howe, C. J.; Wagner, M. J.; Wilce, M. C. *Acta Crystallogr.* **1999**, *D55*, 414−421.
(17) Shibata, N.; Inoue, T.; Nagano, C.; Nishio, N.; Kohzuma, T.; Onodera, K.; Yoshizaki, F.; Sugimura, Y.; Kai, Y. *J. Biol. Chem.* **1999**, *274*, 4225−4230.
(18) Moore, J. M.; Lepre, C. A.; Gippert, J. P.; Chazin, W. J.; Case, D. A.; Wright, P. E. *J. Mol. Biol.* **1991**, *221*, 533−555.
(19) Bagby, S.; Driscoll, P. C.; Harvey, T. S.; Hill, H. A. O. *Biochemistry* **1994**, *33*, 6611−6622.
(20) Badsberg, U.; Jorgensen, A. M. M.; Gesmar, H.; Led, J. J.; Hammerstad, J. M.; Jespersen, L. L.; Ulstrup, J. *Biochemistry* **1996**, *35*, 7021−7031.
(21) Babu, C. R.; Volkman, B. F.; Bullerjahn, G. S. *Biochemistry* **1999**, *38*, 4988−4995.
(22) Banci, L.; Bertini, I.; Luchinat, C. *Nuclear and Electron Relaxation*; VCH: Weinheim, Germany, 1991.

weakly bound Met-Sδ ligand.[23-25] For this type of copper center, the relatively small energy gap between the ground and excited states causes the electronic relaxation times to decrease about 1 order of magnitude,[22,26-28] inducing a corresponding line width narrowing of the NMR signals. Recent advancements in the NMR techniques utilized to investigate these systems have led to the observation and assignment of the ^{1}H NMR signals of metal-bound amino acid residues in oxidized spinach plastocyanin,[29] as well as in other similar blue copper proteins.[30] These signals can be shifted as much as several hundred ppm and have a line width of several hundred kHz ($\sim$600$-$700 ppm at 800 MHz spectrometer frequency). These signals have been observed only using saturation transfer experiments that exploit the favorable electron-exchange rate between the oxidized and the diamagnetic reduced form of the protein.[29,30] Such NMR studies have paved the way toward the complete structural determination of the oxidized form of a blue copper protein in solution by using NMR constraints only. The importance of NMR solution structure determination of the paramagnetic oxidation state of a redox protein relies on the possibility to compare directly its structural and dynamic features with those of its diamagnetic redox counterpart. This is an important research goal per se, and particularly important for blue copper proteins for which X-ray data describing the same protein in two independently crystallized redox states are lacking.

In the present work the copper ligands and donor atoms of a Cu(II)-containing oxidized paramagnetic protein have been identified following the strategy outlined in refs 29 and 30, and its solution structure was obtained using ^{1}H- and ^{15}N paramagnetic NMR spectroscopy. The protein is the recombinant plastocyanin from a cyanobacterium, *Synechocystis* PCC6803. The experimental identification of the copper ligands has been translated into metal-to-donor atom distance constraints and Cu$-$S$-$C$-$H dihedral angles for the coordinated cysteine. 1D NOEs from the hyperfine-shifted signals have been used to frame the donor groups within the protein environment, while T_1 values of protons sensing the paramagnetic effect of the copper(II) ion were used to constrain them in its neighborhood. The obtained structure is compared with the existing X-ray structure of a triple mutant of the same protein.[13] The present article is the first account of a project aimed at describing the structural and dynamic properties of the oxidized and reduced forms of this protein in solution. (After this work was completed, a solution structure of an oxidized blue copper protein was made available in the Protein Data Bank. Although the file is not accompanied by a published paper, it appears that no effort was made to detect and identify signals from the ligand residues, and no hyperfine-based constraints have been used.)

Materials and Methods

Sample Preparation. Protein cloning, overexpression, ^{15}N-labeling, and purification will be described in a subsequent report. The sequence of the purified protein differs from that previously published [31,32] by a Glu$\rightarrow$Asp mutation in the last residue at the C-terminus. Samples for NMR spectroscopy (2$-$3 mM protein) were prepared in 50 mM sodium phosphate buffer (either in 90% H_2O/10% D_2O or in 100% D_2O) at pH 5.2. Buffer exchange was performed by five cycles of concentration/dilution using Centricon cells (Amicon) equipped with a YM1 membrane. Complete oxidation of the protein was obtained by addition of a slight excess of a potassium ferricyanide solution to the sample. The sample was kept under oxygen atmosphere during the NMR experiments.

NMR Spectroscopy Data Acquisition and Processing. NMR experiments were performed on Bruker Avance spectrometers operating at 600 and 800 MHz proton Larmor frequencies. Data acquisition and processing were performed using a standard Bruker software package (XWINNMR).

1D NOE spectra and saturation transfer experiments on hyperfine-shifted signals were recorded on the unlabeled protein in difference mode after selective irradiation of hyperfine-shifted and fast-relaxing resonances. Two reference frequencies were set to the immediate left and right of the irradiated signal, according to the scheme on$-$off (left)$-$on$-$off (right), as previously described.[33,34] Repetition times (acquisition time + relaxation delay) and irradiation times were 50 and 90$-$120 ms, respectively.

1D saturation transfer spectra, carried out in order to detect signals unobservable in the normal ^{1}H NMR spectrum, were performed on the unlabeled protein as previously described.[29] An "on$-$off" scheme was used, where "on" values were varied from 50 to 1500 ppm, and "off" values were positioned symmetrically to the "on" values with respect to either the frequency of the H_2O resonance or the frequency of the signals for which saturation transfer was observed. For these experiments, a 2.5-mm high-power prototype probe was used at 800 MHz.

2D ^{1}H homonuclear TOCSY[35-38] and NOESY[35,39,40] experiments were acquired at 290 and 295 K in phase-sensitive TPPI mode[41,42] using unlabeled plastocyanin. Water suppression was achieved with a WATERGATE sequence.[43] The values for the spin-lock time in TOCSY experiments were 35 and 45 ms, while the mixing time used in NOESY spectra was 25 and 100 ms. The repetition time in 2D spectra ranged between 600 ms and 1.1 s. 2D ^{1}H homonuclear TOCSY and NOESY spectra consisted of 4K data points in the F2 dimension, whereas 700$-$1024 experiments were recorded in the F1 dimension, with 24 to 128 transients per experiment. The spectral window for TOCSY and NOESY spectra was 9800 Hz at 800 MHz in both directions. Raw data were processed using a sine-squared window function shifted by either π/2 or π/3 in both dimensions. A polynomial baseline correction was applied in both directions. Data were always zero-filled in the F1 dimension to obtain matrices with 2K $\times$ 2K data points. The spectra were calibrated assigning a chemical shift of 4.85 ppm to the water signal with respect to DSS at 295 K.

Heteronuclear [1]H$-$^{15}N 2D and 3D NMR experiments using the ^{15}N-enriched protein were carried out in phase-sensitive TPPI mode at 295 K using a 5-mm reverse-detection probe. [15]N chemical shifts were

(23) Malkin, R.; Malmstrom, B. G. *Adv. Enzymol.* **1970**, *33*, 177$-$244.

(24) Fee, J. A. *Struct. Bonding* **1975**, *23*, 1$-$60.

(25) Holm, R. H.; Kennepohl, P.; Solomon, E. I. *Chem. Rev.* **1996**, *96*, 2239$-$2314.

(26) Koenig, S. H.; Brown, R. D. *Ann. NY Acad. Sci.* **1973**, *222*, 752$-$763.

(27) Andersson, I.; Maret, W.; Zeppezauer, M.; Brown, R. D.; Koenig, S. H. *Biochemistry* **1981**, *20*, 3424$-$3432.

(28) Kroes, S. J.; Salgado, J.; Parigi, G.; Luchinat, C.; Canters, G. W. *J. Biol. Inorg. Chem.* **1996**, *1*, 551$-$559.

(29) Bertini, I.; Ciurli, S.; Dikiy, A.; Gasanov, R.; Luchinat, C.; Martini, G.; Safarov, N. *J. Am. Chem. Soc.* **1999**, *121*, 2037$-$2046.

(30) Bertini, I.; Fernandez, C. O.; Karlsson, B. G.; Leckner, J.; Luchinat, C.; Malmstrom, B. G.; Nersissian, A. M.; Pierattelli, R.; Shipp, E.; Valentine, J. S.; Vila, A. J. *J. Am. Chem. Soc.* **2000**, *122*, 3701$-$3707.

(31) Briggs, L. M.; Pecoraro, V. L.; McIntosh, L. *Plant Mol. Biol.* **1990**, *15*, 633$-$642.

(32) Hervas, M.; Navarro, F.; Navarro, J. A.; Chavez, S.; Diaz, A.; Florencio, F. J.; De la Rosa, M. A. *FEBS Lett.* **1993**, *319*, 257$-$260.

(33) Banci, L.; Bertini, I.; Luchinat, C.; Piccioli, M.; Scozzafava, A.; Turano, P. *Inorg. Chem.* **1989**, *28*, 4650$-$4656.

(34) Dugad, L. B.; La Mar, G. N.; Banci, L.; Bertini, I. *Biochemistry* **1990**, *29*, 2263$-$2271.

(35) Braunschweiler, L.; Ernst, R. R. *J. Magn. Reson.* **1983**, *53*, 521$-$528.

(36) Davis, D. G.; Bax, A. *J. Am. Chem. Soc.* **1985**, *107*, 2820$-$2821.

(37) Bax, A.; Davis, D. G. *J. Magn. Reson.* **1985**, *65*, 355$-$360.

(38) Griesinger, C.; Otting, G.; Wüthrich, K.; Ernst, R. R. *J. Am. Chem. Soc.* **1988**, *110*, 7870$-$7872.

(39) Macura, S.; Ernst, R. R. *Mol. Phys.* **1980**, *41*, 95.

(40) Wider, G.; Macura, S.; Kumar, A.; Ernst, R. R.; Wüthrich, K. *J. Magn. Reson.* **1984**, *56*, 207$-$234.

(41) Marion, D.; Wüthrich, K. *Biochem. Biophys. Res. Commun.* **1983**, *113*, 967$-$974.

(42) Marion, D.; Driscoll, P. C.; Kay, L. E.; Wingfield, P. t.; Bax, A.; Gronenborn, A. M.; Clore, G. M. *Biochemistry* **1989**, *28*, 6150$-$6156.

(43) Sklenar, V.; Piotto, M.; Leppik, R.; Saudek, V. *J. Magn. Reson., Ser. A* **1993**, *102*, 241$-$245.

calibrated by assigning a shift of 21.5 ppm to the ^{15}N-enriched $(NH_4)_2$-SO_4 signal at 295 K with respect to liquid ammonia. ^{15}N decoupling during acquisition was achieved by the WALTZ-16 pulse sequence.[44] Both 2D HMQC[45,46] and HSQC[47] spectra were acquired with 2K × 256 data points in the F2 and F1 dimensions, respectively, with 8–32 scans per experiment. The spectral width used in these spectra was 9200 Hz for ^1H, and 3300 Hz for ^{15}N, at 800 MHz. In some experiments, the spectral width for ^{15}N was extended to 8000 and 65000 Hz. 3D WATERGATE TOCSY-HMQC at 600 MHz and NOESY-HMQC at 800 MHz spectra were recorded with 1024 (^1H) × 64 (^{15}N) × 400 (^1H) data points, with eight scans per experiment. The spectral width was set to the smallest possible value including all ^1H- and ^{15}N resonances. Spin-lock and mixing times in 3D TOCSY-HMQC and NOESY-HMQC spectra were 60 and 100 ms, respectively. Processing of the 3D spectra was performed using 1024 (^1H) × 128 (^{15}N) × 512 (^1H) points for both experiments.

Nonselective T_1 values for the hyperfine-shifted signals were measured using the inversion–recovery method.[48] Two series of inversion–recovery ^{15}N HSQC spectra ($180°$–τ–HSQC) were carried out using 500 and 800 MHz spectrometers to determine the nonselective longitudinal relaxation rates ($1/T_1^{eff}$) of backbone HN protons. The values of τ ranged from 1 ms to 1 s in the first series of experiments, while the 1–300 ms range was used in the second series. The repetition time was set to 1 s and 300 ms in the first and second series, respectively. The intensity of each inversion–recovery HSQC cross-peak was plotted as a function of the delay time τ and fitted to the following equation: $I = I^{\infty} \cdot [1 - 2 \cdot \exp(-\tau/T_1^{eff})]$, from which the T_1^{eff} values were obtained.

3D HNHA spectra[49] were collected at 800 MHz to determine the $^3J_{H\alpha-NH}$ coupling constants. The spectra were obtained using 1024(^1H) × 64 (^{15}N) × 128 (^1H) data points, with 16 scans per experiments. States-TPPI was used for quadrature detection in the indirect dimensions.[42,50] The relative intensities of intra- and interresidue Hα–NH NOESY cross-peaks NOESY-HMQC and NOESY spectra were used to obtain additional dihedral angle constraints.[51]

The refocusing time used in all heteronuclear experiments was either 2.5 ms (for detection of paramagnetic connectivities and for the second series of experiments carried out in order to measure T_1 values of NH) or 5.4 ms (in all other cases). The repetition time ranged from 200 ms to 1 s. In the case of ^{15}N-labeled samples, ^{15}N decoupling during acquisition was employed.

Peak Assignment and Structural Constraints. The program XEASY[52] was employed for spectral analysis and for NOESY cross-peaks integration. The sequence-specific resonance assignment was carried out using standard procedures.[53,54]

The volumes of assigned NOESY cross-peaks were transformed into ^1H–^1H upper distance limits using the program CALIBA.[55] Standard calibration was performed using backbone, side-chain, and methyl classes, using a $(1/r)^6$ distance dependence. 1D NOEs were calibrated separately. In particular, the 1D NOEs were classified as either weak or strong. In the first case, an upper distance limit of 5.5 Å was used

for generic protons, while an upper distance limit of 6.5 Å was used for methyl groups. In the case of strong NOEs, an upper distance limit of 3.5 Å was used for both proton and methyl classes.

A total of 28 dihedral angle constraints for ϕ angles were derived by determination of the $^3J_{H\alpha-NH}$ constants from the analysis of 3D HNHA spectra. The $^3J_{H\alpha-NH}$ constants were transformed into ϕ dihedral angle constraints using the Karplus relationship.[56] The ϕ dihedral angles constraints were divided into two classes: for $^3J_{H\alpha-NH}$ constants larger than 8 Hz the ϕ dihedral angle was restrained between $-145°$ and $-75°$, while for coupling constants smaller than 4.5 Hz, the angles were restrained between $-105°$ and $-35°$. Additional 21 ϕ and 47 ψ dihedral angles constraints were obtained from the relative intensities of the intra- and interresidue Hα–NH NOESY cross-peaks as measured in NOESY-HMQC and NOESY spectra.[51] The ϕ ranges $-145°$ to $-75°$, and $-105°$ to $-35°$, and the ψ ranges $-70°$–$0°$ and $100°$–$180°$ were used to constrain residues in the A or B regions of the Ramachandran plot, respectively. The large intensity of the intraresidue Hα–NH NOESY cross-peak for residue Leu-36, together with the inter/intraresidue Hα–NH cross-peak ratio close to 1, prompted us to constrain this residue in the L region of the Ramachandran plot (ϕ: $40°$–$80°$; ψ: $0°$–$70°$).

The peptide bonds for residues Pro-18 and Pro-38 were imposed to be *cis*, as always found in the structures of plastocyanins. This conformation could not be confirmed using the NMR data for the oxidized form of the protein. In fact, no signal for Pro-38 was assigned, probably due to its vicinity to the paramagnetic copper ion, while the degeneracy of the Hα signals for Pro-18 and Glu-17 prevented the distinction between *cis* and *trans* configuration for Pro-18. However, the analysis of the NMR spectra of the reduced form (unpublished data) confirms that both Pro-18 and Pro-38 have *cis* geometry.

Additional constraints were introduced by considering the presence of H-bonds involving peptide amide NH groups and carbonyl oxygen atoms. Such constraints were considered only if the amide ^1H resonance was nonexchanging in 90% D_2O solutions after 10 min, and if the H-bond involving this proton was observed in more than 50% of the structures calculated using DYANA[57] (see below) without inclusion of these constraints. For these cases, the upper and lower distance limits used for the H··O distance were 1.8 and 2.4 Å, respectively. Moreover, the N··O distances were restrained between 2.4 and 3.4 Å. An additional H-bond constraint was introduced between Asn-40 NH and Cys-83 Sγ (see Results section) using the same upper and lower distance limits as above.

The copper atom was included in the structure calculations as a residue bound to the C-terminus of the protein by 33 linker dummy residues, using the procedure implemented in DYANA.[57] These dummy residues are used to let the copper atom move freely during the DYANA run. The number of these residues in the linker is chosen to be large enough to allow the copper atom to get close to any residue in the protein, according to the experimental constraints relative to the copper ion. Bond distance restraints were imposed to the copper coordination using lower and upper distance limits, large enough to allow the metal-bound residues to adopt a conformation in solution that would be consistent with the rest of NMR data. In particular, restraints of 2.0 ± 0.3 and 2.2 ± 0.3, corresponding to normal coordination bonds, were used for Cu–NHis and Cu–SCys, respectively, on account of the large contact interaction experienced by these ligands. The Cu–SMet distance was freely allowed to vary within a larger range (from 2.4 to 3.2 Å), to account for the much smaller contact contribution experienced by this residue. No copper–ligand angle restraints were used at this stage of the calculation.

The C_{α}–C_{β}–S_{γ}–Cu dihedral angle of the Cu-bound Cys residue was constrained between 150° and 210°, as judged from the essentially equivalent hyperfine shifts of the corresponding β-CH_2 protons and from the Karplus-type relationship[29,30] valid for this system (see Results section).

Nonselective longitudinal relaxation times $(T_1^{eff})_{obs}$ of protons lying in the vicinity of the paramagnetic Cu(II) metal ion, as well as protein

(44) Shaka, A. J.; Keeler, J.; Freeman, R. *J. Magn. Reson.* **1983**, *53*, 313–340.

(45) Bax, A.; Griffey, R. H.; Hawkins, B. L. *J. Am. Chem. Soc.* **1983**, *105*, 7188–7190.

(46) Bax, A.; Griffey, R. H.; Hawkins, B. L. *J. Magn. Reson.* **1983**, *55*, 301–315.

(47) Bodenhausen, G.; Ruben, D. J. *Chem. Phys. Lett.* **1980**, *69*, 185–189.

(48) Vold, R. L.; Waugh, J. S.; Klein, M. P.; Phelps, D. E. *J. Chem. Phys.* **1968**, *48*, 3831–3832.

(49) Vuister, G. W.; Bax, A. *J. Am. Chem. Soc.* **1993**, *115*, 7772–7777.

(50) States, D. J.; Habenkorn, R. A.; Ruben, D. J. *J. Magn. Reson.* **1982**, *48*, 286–292.

(51) Gagné, S. M.; Tsuda, S.; Lee, M. X.; Chandra, M.; Smillie, L. B.; Sykes, B. D. *Protein Sci.* **1994**, *3*, 1961–1974.

(52) Bartels, C.; Xia, T.; Billeter, M.; Guntert, P.; Wüthrich, K. *J. Biomol. NMR* **1995**, *6*, 1–10.

(53) Wüthrich, K. *NMR of proteins and nucleic acids*; John Wiley & Sons: New York, 1986.

(54) Arseniev, A.; Schultze, P.; Worgotter, E.; Braun, W.; Wagner, G.; Vasak, M.; Kagi, J. H.; Wüthrich, K. *J. Mol. Biol.* **1988**, *201*, 637–657.

(55) Guntert, P.; Braun, W.; Wüthrich, K. *J. Mol. Biol.* **1991**, *217*, 517–530.

(56) Pardi, A.; Billeter, M.; Wüthrich, K. *J. Mol. Biol.* **1984**, *180*, 741–751.

(57) Guntert, P.; Mumenthaler, C.; Wüthrich, K. *J. Mol. Biol.* **1997**, *273*, 283–298.

backbone HN protons with T_1^{eff} < 200 ms, were transformed into Cu−H distance constraints following a previously established procedure.[58] The paramagnetic contribution to the proton relaxation rate $(1/T_1^{eff})_{para}$ was extracted from the data by subtracting the diamagnetic component $(1/T_1^{eff})_{dia}$ from $(T_1^{eff})_{obs}$. $(1/T_1^{eff})_{dia}$ was estimated to be 2.3 s^{-1} for all protons. This value was calculated by considering the average of all $(1/T_1^{eff})_{obs}$ values smaller than 3.3 s^{-1} and relative to protons located far away from the copper ion. The possible combined effect of amide proton exchange and radiation-damping phenomena has been estimated to be minor as shown by the fact that the longitudinal relaxation rate enhancement of the NH amide protons that undergo the largest saturation transfer from the water signal is modest (data not shown). The distance (d_i) between the copper ion and each proton for which the paramagnetic relaxation rate could be determined was established using the DYANA structure calculated (see below) without these constraints. A plot of d_i versus $[(1/T_1^{eff})_{para}]^{-1/6}$ allowed the identification of a region of points delimited by two straight lines passing through the origin. The two limiting values for the slopes (K_{lower} = 9.57 and K_{upper} = 13.16 Å s$^{-1/6}$) were then used to set the lower and upper distance limits for each proton.

Structure Calculation. Structures were calculated by simulated annealing-torsion angle dynamics (TAD) carried out using DYANA.[57] The calculations started from 400 randomly produced conformers, each of them being subjected to 8000 TAD steps to adapt its conformation to the distance constraints. The stereospecific assignments (19 in total) were obtained using GLOMSA.[55] Few cycles of (i) structure calculation and (ii) recalibration using CALIBA, yielded an ensemble of structures satisfying the experimental constraints. The best 35 structures, having a target function smaller than 0.6 Å^2, were selected as a single family for further analysis.

Structure Refinement. The mean structure from the DYANA family was calculated using MOLMOL[59] and subjected to restrained energy minimization (REM) using the SANDER module of the AMBER 5.0 program package.[60] The force field parameters for all residues, excluded those for the copper-coordinated ligands, were the standard AMBER "all-atoms" parameters. The calculations were performed in vacuo with the distance-dependent dielectric constant option. The nonbonded interactions were evaluated with a cutoff of 10 Å. The mixed linear-harmonic flat-bottomed potential implemented in SANDER was applied to all structural constraints. This potential involves a null force constant for structural constraints within the allowed limits, a nonzero harmonic force constant in a small interval outside the allowed limits, and a linearly dependent potential beyond that limit.

NOE-derived distance constraints were restricted below the upper distance limit (r_i), using a force constant of 32 kcal mol^{-1} Å^{-2} for the interval r_i + 0.5 Å. Distance constraints involving the same H-bonds used for DYANA calculations were included in the REM calculation, restricting the NH···O and N···O distances to the same upper (r_i) values used in DYANA, with a force constant of 32 kcal mol^{-1} Å^{-2} for the range r_i + 0.5 Å. The Cu−H distances derived from the analysis of the nonselective longitudinal relaxation rates were also restrained to the same upper (r_i) limits used in DYANA, with a force constant of 32 kcal mol^{-1} Å^{-2} for r_i + 0.5 Å.

The Cu−NHis and Cu−SCys distances were constrained at 2.1 ± 0.1 and 2.2 ± 0.1, respectively, using a linear-harmonic flat-bottomed potential with force constants of 50 kcal mol^{-1} Å^{-2} in the 0.3-Å distance ranges below and above these limits. The Cu−SMet distance was analogously constrained within the 2.75 ± 0.05 Å range, using a force constant of 40 kcal mol^{-1} Å^{-2}. The Cu−N(His)−Cγ, Cu−N(His)−Cϵ, Cu−S(Cys)−Cβ, Cu−S(Met)−Cγ, and Cu−S(Met)−Cϵ angles were restrained around 127 ± 0°, 127 ± 0°, 105 ± 5°, 130 ± 10°, and 110 ± 10°, respectively, using a linear-harmonic flat-bottomed potential

(58) Bertini, I.; Couture, M. M. J.; Donaire, A.; Eltis, L. D.; Felli, I. C.; Luchinat, C.; Piccioli, M.; Rosato, A. *Eur. J. Biochem.* **1996**, *241*, 440−452.

(59) Koradi, R.; Billeter, M.; Wüthrich, K. *J. Mol. Graphics* **1996**, *14*, 51−55.

(60) Pearlman, D. A.; Case, D. A.; Caldwell, J. W.; Ross, W. S.; Cheatham, T. E.; Ferguson, D. M.; Seibel, G. L.; Singh, U. C.; Weiner, P. K.; Kollman, P. A. *Amber 5.0*; University of California: San Francisco, 1997.
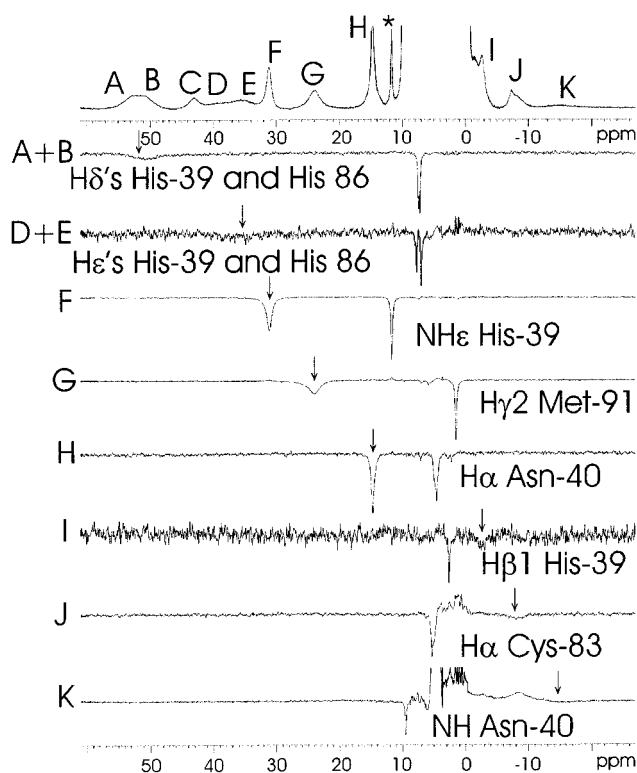

Figure 1. 800 MHz ^{1}H NMR spectra at 295 K of oxidized *Synechocystis* PCC6803 plastocyanin (50 mM phosphate buffer, pH 5.2 in H$_2$O). The asterisk indicates a resonance belonging to the reduced form. The top panel reports the 1D spectrum, while the lower panels show 1D saturation transfer experiments obtained upon saturating the indicated signals at the positions shown by arrows. The assignment of the signals is indicated.

with force constants of 50 kcal mol^{-1} deg^{-2} in the 50° ranges below and above the given values. Analogously, the (His)N−Cu−N(His), (His)N−Cu−S(Cys), (His)N−Cu−S(Met), and (Met)S−Cu−S(Cys) angles were restrained in the 110 ± 10°, 125 ± 15°, 95 ± 15°, and 100 ± 10° range with a force constant of 20 kcal mol^{-1} deg^{-2} in the 50° angle ranges below and above these limits.

The quality of the structure was checked using PROCHECK.[61] The coordinates of the structure family and the minimized DYANA mean structure have been deposited in the PDB (code 1I0W, 1I0Y).

Results

^{1}H NMR Spectral Assignment of Oxidized Plastocyanin. *Synechocystis* PCC6803 plastocyanin was overexpressed in *Escherichia coli* to obtain large amounts of ^{15}N-enriched protein necessary to overcome the problem of resonance overlapping and to facilitate the ^{1}H and ^{15}N signal assignment. The 800 MHz ^{1}H NMR spectrum (Figure 1) shows eight downfield and three upfield hyperfine-shifted signals (Table 1) which obey Curie temperature dependence (decrease in shift with increasing temperature) as predicted for systems containing a single paramagnetic metal ion. Two signals (C and F) appear to be exchangeable, as they were not observed in the spectrum recorded in deuterated water. All hyperfine-shifted signals are characterized by very short longitudinal and transverse nuclear relaxation times. Analysis of the relative signal intensities indicates that each signal accounts for one proton. The ^{1}H NMR assignment of the hyperfine-shifted signals was carried out through 1D saturation transfer experiments performed on samples containing about equal amounts of the oxidized and

(61) Laskowski, R. A.; MacArthur, M. W.; Moss, D. S.; Thornton, J. M. *J. Appl. Crystallograph.* **1993**, *26*, 283−291.

Table 1. Summary of ^{1}H NMR Data on Hyperfine-Shifted Signals of Oxidized Plastocyanin from *Synechocystis* PCC6803

proton type (label in spectrum)	angle ϑ (deg)^a	Cu−H distance (Å)^a	δ_{obs} (ppm)	δ_{dia} (ppm)	δ_{dip} (ppm)	δ_{con} (ppm)	A_c (MHz)
			His 39				
Hα (Z)	146	2.9	+19.2	+6.0	+5.6	+7.6	+0.3
Hβ1 (I)	109	4.6	−2.7	+2.6	−0.9	−4.4	−0.2
Hβ2	101	3.2			−3.5		
Hδ2 (B)	102	5.2	+51.1	+7.4	−0.8	+44.5	+1.6
Hϵ1 (E)	70	3.1	+35.7	+7.0	−2.8	+31.5	+1.1
NHϵ2 (F)	86	5.0	+31.1	+11.7	−1.0	+20.4	+0.7
			Asn 40				
NH (K)	117	4.1	−15.2	+9.5	−0.7	−24.0	−0.9
Hα (H)	118	6.8	+14.7	+4.5	−0.1	+10.3	+0.4
			Cys 83				
Hα (I)	92	4.9	−7.8	+5.3	−1.1	−12.0	−0.4
Hβ1 (X)	63	3.2	+614	+3.5	−1.5	+612	+21.9
Hβ2 (Y)	65	3.4	+517	+3.0	−1.5	+516	+18.4
			His 86				
Hα	88	5.4			−0.8		
Hβ1	67	2.8			−3.2		
Hβ2	64	4.1			−0.8		
Hδ2 (A)	99	5.2	+52.6	+7.2	−0.9	+46.3	+1.7
Hϵ1 (D)	124	3.2	+38.5	+7.7	−0.2	+31.0	+1.1
NHϵ2 (C)	116	5.0	+42.9		−0.4		
			Met 91				
Hα	20	6.6			+0.7		
Hβ1	30	4.6			+1.7		
Hβ2	40	4.3			+1.2		
Hγ1	26	4.4			+2.2		
Hγ2 (G)	5	4.7	+24.0	+1.5	+2.5	+20.0	+0.7
ϵ−CH$_3$	34	3.9			+2.3		

^{a} These parameters were obtained using the X-ray structure of oxidized *Synechocystis* PCC6803 plastocyanin (PDB code 1PCS).[13]
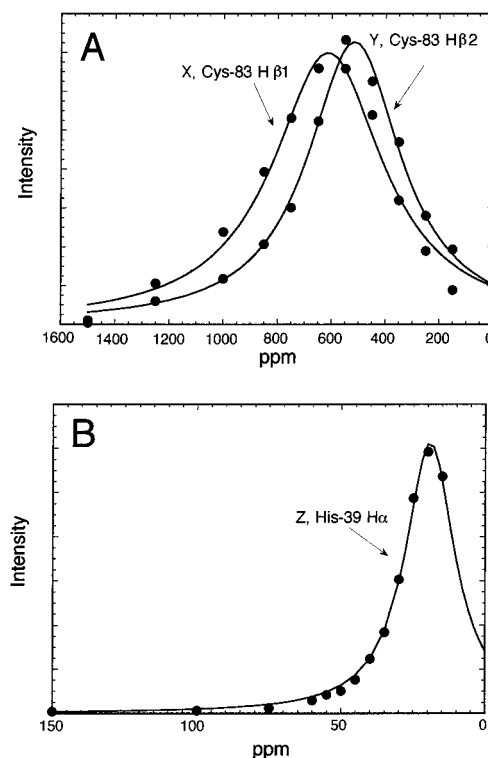

Figure 2. Positions and line widths of the ^{1}H NMR signals not observable in the normal spectrum of oxidized *Synechocystis* PCC6803 plastocyanin. The profiles of signals X, Y (panel A), and Z (panel B) were obtained using saturation transfer experiments (see Experimental Section and Results and Discussion) by plotting the intensity of the respective exchange connectivities with the reduced species as a function of the downfield decoupler irradiation frequency, and performing a Lorentzian fit to the points obtained.

reduced forms of the protein. This was done in combination with 2D TOCSY and NOESY spectra of the reduced protein, following a procedure described previously.[29] Saturation of signal C did not afford any signals in the diamagnetic region using the reported experimental conditions. On the basis of the solvent exchangeability of the corresponding proton and its NMR properties (chemical shift and line width) this signal could be tentatively assigned to His-86 Hϵ2. This signal is not observed in the reduced form probably because the small chemical shift separation between this signal and the water resonance (as compared to the oxidized form) brings the signal in the reduced form in the fast exchange limit situation. The full assignment of the hyperfine-shifted signals will not be discussed as largely coincident with that already described for the case of spinach plastocyanin.[29] It is noteworthy to point out that, in analogy with the spinach case, also in *Synechocystis* PCC6803 plastocyanin the amide NH proton of Asn-40 (signal K) experiences a chemical shift that cannot be explained only by dipolar interaction with the Cu(II) ion, but rather by the presence of a significant electron spin density on the nucleus coming from contact interactions. The latter could be propagated from the copper ion to the Asn-40 NH proton through an H-bond with the copper-bound Cys-83 Sγ atom. This hypothesis could be verified using simple calculations at the semiempirical PM3 level, performed using the program SPARTAN,[62] that showed how a single molecular orbital is obtained by combination of the Cu(II) $d_{x^2-y^2}$, the Cys-83 Sγ p_x (or p_y) orbital, as well as the Asn-40 amide nitrogen sp^2 orbital. This result has led to inclusion of the H-bond between the mentioned atoms as a structural constraint. It is also important to notice that the

chemical shift observed for signal K (−15.2 ppm) is very similar to that observed for the same proton in oxidized spinach plastocyanin (−19.0 ppm).[29] In the latter case the signal was identified using blind saturation transfer experiments, while in the present case it was directly observed, therefore strengthening the methodology proposed to detect unobservable very broad signals.

To detect the signals of the β-CH$_2$ protons of the Cu(II)-bound cysteine, broadened beyond detection because of the large direct electron spin delocalization observed in plastocyanins,[63−65] a "saturation transfer profile" experiment was carried out as previously described.[29] High power irradiation of a sample containing a ~50:50% mixture of oxidized and reduced protein, sampling a very large spectral window (from +1500 to −1500 ppm) in steps of 50−100 ppm, resulted in the observation of the build-up and decay of the intensity of the corresponding signals of the reduced protein. In this way, the positions of signals X (at 614 ppm) and Y (at 517 ppm) for Cys-83 β-CH$_2$ in the oxidized protein could be obtained (Figure 2A). The very large line width of these signals (~400 and 330 kHz, respectively), determined using a Lorentzian fit to the curves shown in Figure 2, prevent their direct observation in the 1D ^{1}H NMR spectrum. The presence of additional broad signals in the near downfield and upfield regions of the spectrum was checked by performing a similar saturation transfer profile using lower

(62) *MACSPARTAN-PLUS*; *Wavefunction, Inc., 18401 Von Karman Ave. Ste. 370, Irvine, CA 92612.*

(63) Werst, M. M.; Davoust, C. E.; Hoffman, B. M. *J. Am. Chem. Soc.* **1991**, *113*, 1533−1538.

(64) Shadle, S. E.; Penner-Hahn, J. E.; Schugar, H. J.; Hedman, B.; Hodgson, K. O.; Solomon, E. I. *J. Am. Chem. Soc.* **1993**, *115*, 767−776.

(65) George, S. J.; Lowery, M. D.; Solomon, E. I.; Cramer, S. P. *J. Am. Chem. Soc.* **1993**, *115*, 2968−2969.

Table 2. Summary of NMR Constraints Used for DYANA Structure Calculation, Restraint Violations, Structural Statistics, and Energetics for the Restrained Energy-Minimized DYANA Mean Solution Structure of Oxidized Plastocyanin from *Synechocystis* PCC6803

structural constraints	total	violations	rms violation (Å)
meaningful (total) NOESY	1041 (1450)	67	0.023
NOE	18		
overall intraresidue	162	10	0.023
overall sequential	273	32	0.028
overall medium range[a]	130	3	0.020
overall long range	494	22	0.020
T_1	26	0	-
ϕ	49	6	0.265[b]
ψ	47	3	0.248[b]
χ_2	1	0	0
H-bonds	18	1	0.003
copper ligand distances	4	1	0.012
overall total	1204	69	0.022
overall violations larger than 0.3 Å		0	
overall violations between 0.1 and 0.3 Å		17	
target function (Å²)	0.66		
AMBER average total energy (kJmol⁻¹)	−992.52		
	Structure Analysis[c]		
% of residues in most favored regions	79.3		
% of residues in allowed regions	20.7		
% of residues in generously allowed regions	−		
% of residues in disallowed regions	−		
no. of bad contacts/100 residues[d]	−		
H-bond energy (kJ mol⁻¹)[d]	0.7		
overall *G*-factor[d]	−0.36		

[a] Medium-range distance constraints are those between residues $(i,i+2)$, $(i,i+3)$, $(i,i+4)$, and $(i,i+5)$. [b] Degrees, not included in total. [c] According to the Ramachandran plot. [d] The program PROCHECK was used to check the overall quality of the structure. According to the PROCHECK statistic, less than 10 bad contacts per 100 residues, an average hydrogen-bond energy in the range 2.5−4.0 kJ mol⁻¹, and an overall *G*-factor larger than −0.5 are expected for a good quality structure.[61]

irradiation power and finer sampling (5 ppm, with "off" irradiation placed symmetrically with respect to the residual water signal). The additional broad signal Z̲ was thus detected (Figure 2B), centered at 19.2 ppm, with a line width of 16.8 kHz, and subsequently assigned to His-39 Hα .

The ¹H and ¹⁵N NMR signals of protein residues not directly bound to Cu(II) and located at distances larger than ∼5 Å, and thus not strongly influenced by the presence of the paramagnetic Cu(II) ion, have been partially or completely assigned in the oxidized protein using classical techniques exploiting the availability of both 2D and 3D homo- and heteronuclear spectra. In particular, 75% of the total number of ¹H and ¹⁵N signals resonances were assigned, and the full ¹H and ¹⁵N assignment achieved in this study, together with the stereospecific assignment, is reported in Table 1 of Supporting Information.

Structure Calculation. Table 2 reports the details of the experimental observables used for structure calculation, while Figure 3 shows the summary of the sequential and medium-range NOE connectivities involving NH, Hα, and Hβ protons. Figure 4 reports the distribution of the meaningful NOEs per residue as well as the residue-by-residue experimental constraints used for the calculation. As follows from this figure, a series of strong sequential $d_{H\alpha-NH}$ connectivities were observed for this protein. These connectivities, together with (i) several $^3J_{H\alpha-NH}$ constants larger than 8 Hz, (ii) a value smaller than unity for many intra/interresidue Hα−NH cross-peak ratios, and (iii) the presence of slowly exchangeable amide protons unambiguously indicate that, as expected, the secondary structure of the protein is largely characterized by the presence of β-sheets. The detection of $d_{H\alpha-NH}(i,i+3)$ as well as $d_{H\alpha-H\beta}(i,i+3)$ connectivities for amino acids 50−56 suggests the presence of an α-helix in this region. The small values of $^3J_{H\alpha-NH}$ constants determined for these residues, together with a value larger than unity for their intra/interresidue Hα−NH cross-peak ratios, further confirm this indication. In the DYANA structure

calculation the copper−ligand distances were loosely constrained around values typically observed for plastocyanins.

The 35 DYANA structures generated by TAD calculations and having the lowest target function (<0.6 Å²) have no consistent violations, have no residual violation exceeding 0.3 Å, and experience global root-mean-square deviation (rmsd) from the mean structure of 0.72 ± 0.14 and 1.16 ± 0.17 Å for the backbone and heavy atoms, respectively. The distribution of the final rmsd per residue for the DYANA family is reported in Figure 5, while a "sausage" stereoview of the backbone for the DYANA family is shown in Figure 6A. The diameter of the "sausage" is proportional to the local backbone rmsd value.

The mean structure of the DYANA family was subjected to an energy minimization process using the AMBER force field. The Cu−L distances were more tightly constrained, around the mean values of the DYANA family, during the energy minimization, and additional constraints on the coordination angles were included. In this process, the copper coordination constraints were left loose enough (and looser than in previous structural studies on copper-containing metalloproteins[18−21]) as not to bias the chromophore to adopt a particular geometry (e.g., either regularly trigonal or regularly tetrahedral).

The structure quality parameters for the restrained energy-minimized mean structure are reported in Table 2. The total number of meaningful constraints, the relatively small number and size of the violations, the distribution of backbone dihedral angles in the Ramachandran plot, as well as the overall *G*-factor (as defined in ref 61), indicate that the quality of the structure is comparable to that of solution structures of diamagnetic proteins.

Discussion

Oxidized *Synechocystis* PCC6803 plastocyanin shows several hyperfine-shifted signals whose isotropic chemical shift is
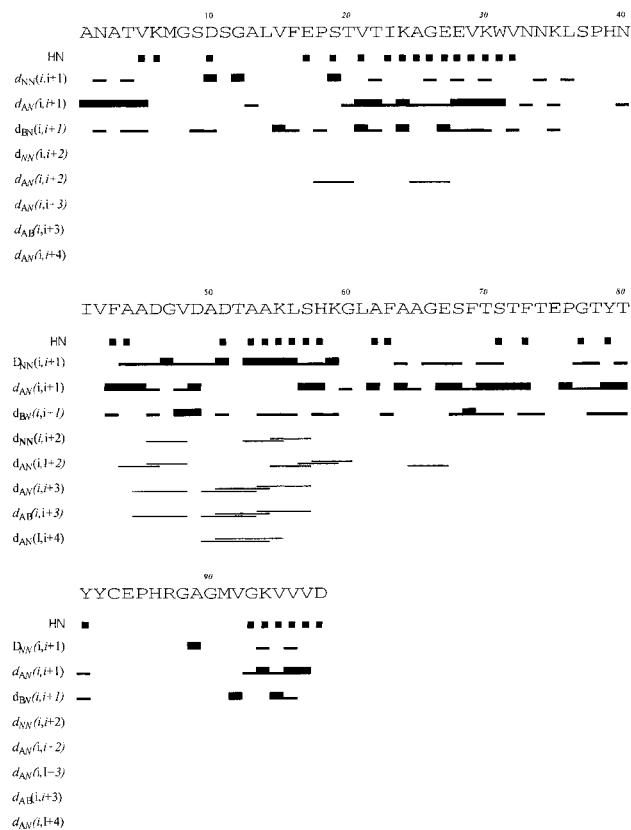
Figure 3. Schematic plot of sequential and medium-range NOEs involving NH, Hα, and Hβ protons in oxidized *Synechocystis* PCC6803 plastocyanin. The thickness of the bar represents the intensity of the NOESY cross-peaks. The slowly exchanged NH protons are indicated in the upper panel. The symbols $d_{XY}(i,i+j)$ indicate the connectivity between the proton attached to atom X (backbone nitrogen N, α-carbon A, β-carbon B) and the proton attached to atom Y; the symbol i indicates the sequential amino acid numbers, and j is the distance in sequence from the ith amino acid.

composed of the Fermi contact shift, the pseudocontact shift (or rotational average of the dipolar shift), and the diamagnetic shift.[29] The latter is available from the spectrum of the reduced form (unpublished data). The separation of the other contributions was performed as described previously,[29] and the results of these calculations are shown in Table 1. As expected, the estimated pseudocontact contribution to the observed chemical shifts is rather small, while, in analogy to spinach plastocyanin[29] and other blue copper proteins,[30] the contact shift is by far the major contribution. The hyperfine coupling constants, calculated from the contact contribution to the hyperfine shifts (Table 1), are largely coincident with those previously calculated for oxidized spinach plastocyanin.[29] This result confirms that, for this type of copper center, a large fraction of unpaired spin density is delocalized over the metal-bound cysteine residue.

Signal detection in Cu(II) proteins (signal line widths) depend on both dipolar and contact contributions to transverse relaxation through the relationship $\Delta\nu = 1/(\pi T_2)$. In turn, dipolar relaxation depends on the reciprocal of the sixth power of the metal–nucleus distance, while contact relaxation depends on the square of the hyperfine-coupling constant. Both depend on the electronic relaxation time of the metal, which, in the case of Cu(II) plastocyanin, is the dominant correlation time. It has been previously established[29] that, in plastocyanins, NMR signals from residues noncoordinated to Cu(II) centers and experiencing only dipolar broadening, should not be too difficult to observe. Therefore, despite the prohibitively large line widths of the
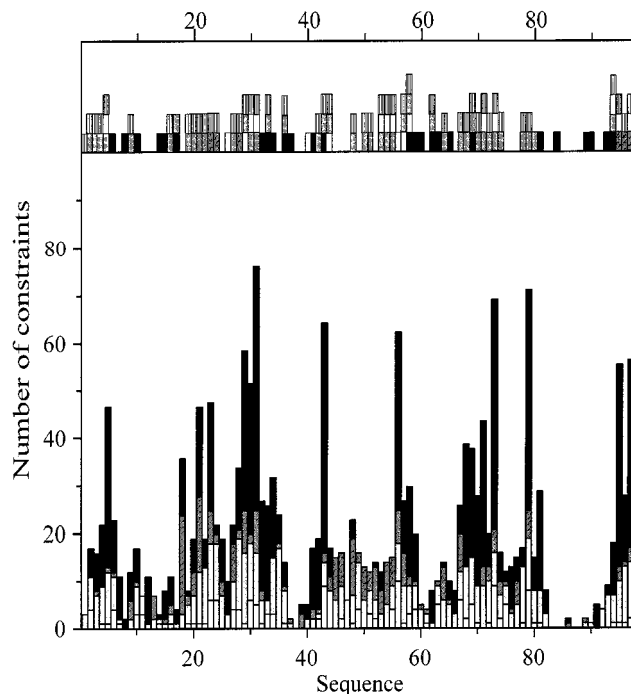

Figure 4. Distribution of meaningful NOEs per residue, used for structure calculation of oxidized *Synechocystis* PCC6803 plastocyanin. Intraresidual, sequential, medium-range, and long-range NOE constraints are in white, light gray, dark gray, and black, respectively. In the top panel the constraints, other than NOEs, used for the calculation (T_1, black bars; H-bonds, white bars; ϕ dihedral angle constraints, gray bars; ψ dihedral angle constraints, dashed bars) are also reported.
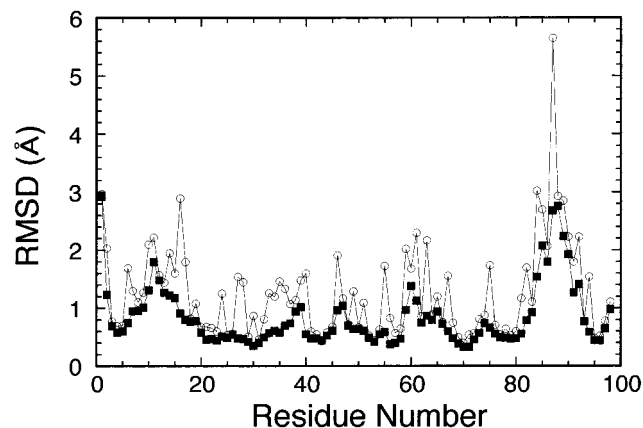

Figure 5. Diagram of global backbone (■) and heavy atoms (○) pairwise rmsd per residue for the 35 DYANA structures of oxidized *Synechocystis* PCC6803 plastocyanin.

signals from the coordinated residues and the relatively unfavorable electronic relaxation properties of the copper(II) ion, a solution structure determination seemed affordable, and it has been indeed successful.

The difficulties of the structure determination in the vicinity of the copper ion have been partially overcome by performing NMR experiments tailored for detection of fast relaxing paramagnetic signals. In addition, paramagnetic effects by themselves did provide additional constraints. First, the very same observation of extremely large contact shifts from the cysteine and histidine ligands, and of a sizable contact shift for a Met-91 Hγ proton, allowed us to impose four experimentally validated coordination bond constraints. Although this is a small number, this type of constraint is extremely valuable, as they are long-range constraints that play the same role as that played
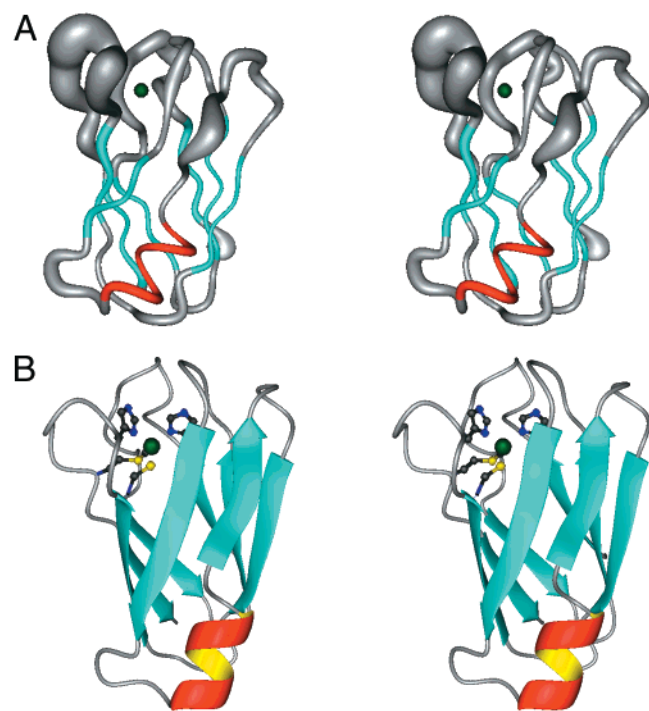
Figure 6. MOLMOL[59] stereo representations of: (A) the "sausage" diagram of the superimposed 35 DYANA backbone structures of oxidized *Synechocystis* PCC6803 plastocyanin; (B) the restrained energy-minimized DYANA mean structure of oxidized *Synechocystis* PCC6803 plastocyanin, showing the elements of secondary structure in different colors. The copper atom is shown in green at the top of the model. The four ligands (His39, Cys83, His86, and Met91) are represented as ball-and-stick colored according to the CPK code.

Figure 7. MOLMOL[59] stereo representation of the backbone atoms of the restrained energy minimized mean DYANA structure (blue) superimposed onto the X-ray structure (orange) of the oxidized triple mutant (PDB code 1PCS).

Figure 8. Plot of the global backbone (■) and heavy atoms (○) rmsd per residue for the restrained energy-minimized DYANA mean structure of oxidized *Synechocystis* PCC6803 plastocyanin vs the solid-state structure of the corresponding triple mutant (PDB code 1PCS).

by disulfide bonds. Second, additional structural information has been obtained by exploiting (i) the distance constraints derived from the determination of the paramagnetic longitudinal relaxation rates of protons located close to the metal ion and (ii) the constraint on the copper-bound cysteine χ_2 angle, derived from the previously determined[29] Karplus-type relationship between this angle and the contact shift experienced by the β-CH$_2$ protons. These paramagnetism-derived structural constraints provided an NMR structure family featuring an acceptably good structural quality even in the neighborhood of the paramagnetic metal ion (see below).

As far as the overall structural features are concerned, the restrained energy minimized DYANA mean structure of oxidized *Synechocystis* PCC6803 plastocyanin (Figure 6B) reveals the common overall fold expected for plastocyanins. The typical eight-stranded β-sandwich structure arranged in two twisted β-sheets, classified as described by Freeman et al.,[9] are observed. β-Sheet-I consists of strands S1 (residues 3−6), S2A (16−17), S3 (28−32), and S6 (69−72), while β-sheet-II contains strands S2B (residues 20−23), S4 (β-bulge, 39−44), S5 (β-bulge, 58−62), S7 (78−82), and S8 (93−97). One α-helix is also present between residues 50 and 56.

The copper site is located at the "northern" end of the molecule, and arranged in a distorted trigonal coordination environment, consisting of His-39, Cys-83, and His-86 pseudoequatorial ligands, plus a weak axial ligand (Met-91), typical of all plastocyanins. The local backbone (and heavy atom) pairwise rmsd values of the copper ligands (better suited than the global rmsd for a study of the local conformation of the protein) are 0.37 (1.14), 0.47 (1.43), 0.72 (2.09), and 0.62 (1.32) Å for His-39, Cys-83, His-86, and Met-91, respectively (Figure 5). The relatively high values for His-86 are due to the large
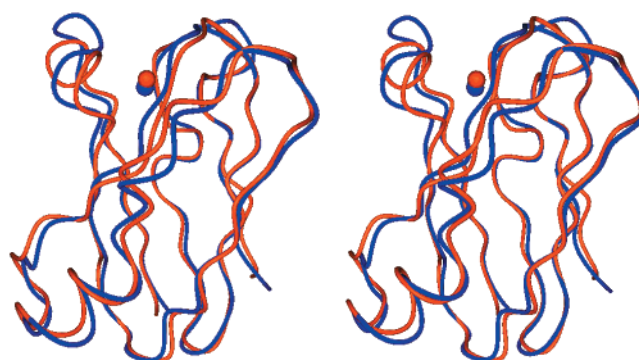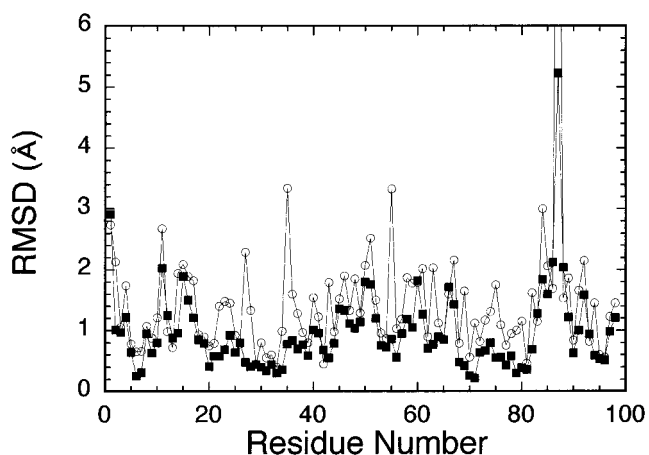
local rmsd for the nearby Arg-87 (0.80 Å), for which only few structural constraints were measured (see Figure 4), mainly because of the proximity of the loop supporting these residues to the paramagnetic center. Overall, such values are not exceedingly higher that those observed in other parts of the structure and show that the resolution is fairly good also around the paramagnetic metal ion.

Figure 7 shows the superposition of the energy-minimized NMR-derived structure with the crystallographic structure of the triple mutant (A44D/D49P/A62L).[13] The overall backbone rmsd between the two structures is 1.13 Å (which compares with a value of 1.03 Å for the pairwise rmsd within the DYANA family), while the corresponding global rmsd per residue are shown in Figure 8. The segments involved in the three mutations that could, in principle, bear structural differences, that is, those around positions 44, 49, and 62 are not characterized by a particularly large global backbone rmsd (0.79, 1.14, and 0.71 Å, respectively). On the other hand, the largest deviation (5.23 Å) is observed for Arg-87, consistent with the very high backbone rmsd of this residue in the NMR family. Two additional large values of the rmsd are observed at positions 11 and 15, i.e., in another loop close to the metal ion. The structure is obviously less well constrained in the neighborhood of the metal ion (cf. Figure 4), even though the use of NMR-derived paramagnetic constraints substantially mitigates the uncertainty. Indeed, the local backbone (heavy atoms) rmsd values between the NMR and X-ray structures for the coordinated residues are 0.27 (0.90), 0.28 (1.15), 0.73 (2.85) and 0.31

(0.83) Å for His-39, Cys-83, His-86, and Met-91, respectively. These local rmsds are smaller (or comparable, for His-86) than the local rmsd within the NMR family discussed above. Therefore, we can conclude that the solution structure provides an essentially accurate description also of the metal site, albeit with lower precision.

Concluding Remarks

The accomplishments of the present work are summarized here below:

(1) ^{1}H NMR spectra (800 MHz) of recombinant ^{15}N-enriched oxidized *Synechocystis* PCC6803 plastocyanin were recorded, and relatively sharp hyperfine-shifted signals were observed. The complete assignment of these signals was performed using 1D and 2D NMR experiments tailored for detecting fast relaxing signals.

(2) The β-CH$_2$ proton signals for the coordinated cysteine residue were detected by devising a "blind" saturation transfer experiment that exploited the favorable electron-exchange properties between oxidized and reduced protein.

(3) The contact hyperfine coupling constants for protons belonging to the copper(II)-bound protein residues were calculated from the contact shifts, and insights in the electronic structure of the system were gained.

(4) The first solution structure of an oxidized Cu(II)-containing protein was determined by exploiting the presence of the paramagnetic metal ion in addition to advanced techniques of NMR structure determination and refinement. This result represents a fundamental breakthrough, which should encourage further investigations of the structure and dynamics of other metalloproteins with similarly unfavorable properties.

Supporting Information Available: Table of ^{15}N and ^{1}H NMR chemical shifts (PDF). This material is available free of charge via the Internet at http://pubs.acs.org.

JA0033685